Raman Scattering

SERS Effects in Silver-Decorated Cylindrical Nanopores

*Rajesh Kodiyath, Jian Wang, Zachary A. Combs, Sehoon Chang, Maneesh K. Gupta, Kyle D. Anderson, Richard J. C. Brown, and Vladimir V. Tsukruk**

Surface-enhanced Raman scattering (SERS) shows great potential for monitoring the chemical composition, internal stresses, and for the trace detection of hazardous molecules that are difficult to detect by other experimental techniques.[1–8] SERS has become an area of intense research as a highly sensitive probe for the trace level detection of small organic molecules since the demonstration of single-molecule detection.[9–13] In order to realize the potential advantages of this approach there have been various designs of SERS-active substrates. The most popular designs involve various engineered substrates, such as roughened metal substrates and metal nanoparticle films,[14,15] metallic and bimetallic nanostructures,[16–24] and porous or holey substrates.[25–28] However, for cutting-edge practical applications of SERS-active substrates the sensitivity of the planar metal structures remains rather low due to the limited density of hot spots available within the laser-activated footprint.[29,30]

3D SERS substrates have been recently introduced to overcome this limitation. These substrates have the potential to increase the level of enhancement for practical SERS detection due to the unique properties they provide in comparison to traditional planar substrates.[26,31] By extending the SERS substrates into the third dimension a much greater surface area for particle coverage compared with traditional substrates may be realized.[32,33] 3D SERS substrates include photonic crystal fibers,[34] porous membranes with cylindrical nanopores,[35] and periodic nanohole arrays.[36] Their high enhancement allows for the ultrasensitive detection of non-resonant molecules.[37]

Several efforts have been made to fabricate 3D SERS substrates by assembling nanoparticles via non-lithographic techniques.[16] The particle distribution in these substrates is not as homogeneous as those observed for substrates fabricated using microfabrication[38] and nanofabrication[39] techniques. However, directed assembly avoids the high cost of fabricating nanostructures via electron beam lithography (many thousands of dollars compared to just a few dollars for assembled nanoparticles). Furthermore, directed assembly overcomes the limitation of the relatively low surface area associated with structures fabricated from lithographic techniques.[40] Even though the enhancement factors for microfabricated substrates are higher than for regular planar substrates, common values average only around 10^7.[41] Therefore, microfabricated lithographical substrates, which are important for fundamental studies, are not promising for practical applications with their current characteristics being a tremendous unresolved roadblock for further utilization.

Porous alumina membranes (PAMs) with long cylindrical nanopores decorated with metal nanoparticles are among the potential candidates for 3D SERS substrates, which exhibit extremely high enhancements owing to their optical transparency and large specific surface area.[29,37] Moreover, open cylindrical pores facilitate the transport of analytes (gases and fluids) that is important for practical analysis. In addition, the incident beam can be directed deeper into the substrate through the waveguiding properties of the nanopores (50–400 nm in diameter) facilitating further Raman signal enhancements.[42,43] Several high-efficiency PAM-based SERS substrates have already been reported, but their general design principles have not been well established.[29,37,44–47] It has only been suggested that the transmission of incident light through the holey substrates and the proper placement of metal nanoparticles inside the pores play a vital role in achieving the highest efficiency, which is critical for the ultrasensitive detection of biological and chemical species.

In this study the role of light transmission and its interaction with metal nanoparticles within cylindrical nanopores of different diameters is investigated, and general guidelines for the design of nanoporous substrates with high SERS activity are presented. Specifically, simulations and experimental studies of substrates with different pore sizes decorated with in situ grown silver nanoparticles bound to the pore walls is shown. We observed that SERS substrates with pore diameters of 355 nm facilitate enhanced light transmission as well as nanoparticle aggregation, which results in greatly improved SERS activity. An enhancement factor of 10^{10}, which is dramatically higher than that for traditional 2D substrates, was observed in this system. Electromagnetic simulations of silver nanoparticle dimers placed at different pore depths confirmed the experimentally observed pore diameter dependence. These simulations coupled with experimental results suggested that nanopore diameters of around 400 nm, the incorporation of the nanoparticle dimers within the first 10 μm beneath the surface, and keeping the light transmittance

Dr. R. Kodiyath, Z. A. Combs, Dr. S. Chang, M. K. Gupta, K. D. Anderson, Prof. V. V. Tsukruk
School of Materials Science and Engineering
Georgia Institute of Technology
Atlanta, GA, USA
E-mail: vladimir@mse.gatech.edu
Dr. J. Wang, Dr. R. J. C. Brown
Analytical Science Division
National Physical Laboratory
Teddington, Middlesex, TW11 0LW, UK

DOI: 10.1002/smll.201101936

small NANO MICRO

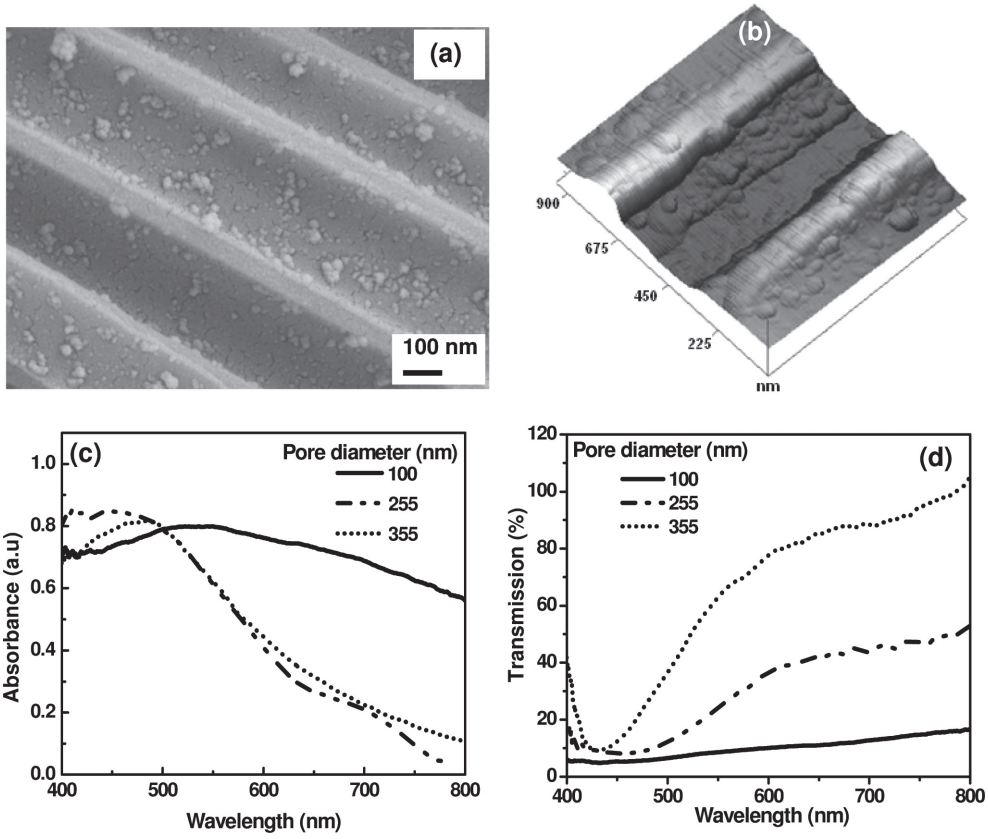

Figure 1. SEM (a) and AFM (b) images of silver nanoparticles grown in porous alumina membranes with 355 nm pore diameters. UV–vis absorption (c) and transmission spectra (d) of SERS substrates with different pore diameters.

above 50% are all critical to achieve SERS substrates that show enhancement factors exceeding 10^{10} for the selected benchmark Raman marker, benzenethiol (BT). The observed record enhancement factor is four orders of magnitude better than that commonly reported for this marker on 2D substrates of gold and silver nanostructures.[48–50]

In order to systematically study the effect of pore diameter on the SERS activity, PAMs with different pore diameters ranging from 100 to 355 nm were synthesized[51,52] following a two-step anodization process (Figure S1, Supporting Information (SI)). In this study an in situ electroless-deposition growth method[53] to obtain a uniform distribution of silver nanoparticles on the pore walls was employed. High-resolution scanning electron miscroscope (SEM) images of the fractured substrates with pore diameters of 355 nm show a distribution of immobilized silver nanoparticles on the inner walls (**Figure 1**a) (see data for 100 nm and 255 nm pores in the SI, Figure S2). The particles with smaller sizes that can be seen on the pore walls are the initial silver seeds with diameters around 5 nm. It was demonstrated earlier that PAMs decorated with silver seeds did not show significant SERS activity.[53] The size of the grown silver nanoparticles is 30 ± 10 nm as estimated from the atomic force microscopy (AFM) and SEM images (Figure 1b, Figure S3, SI). Although for smaller pore diameters predominantly individual nanoparticles are observed, PAMs with larger pore diameters facilitate the aggregation of silver nanoparticles on the pore walls, which predominantly exhibit dimers (about 60 nm) in addition to individual nanoparticles (Figure S2 and S3, SI).

The optical absorption centered at 486–530 nm for the nanoparticle-decorated PAM substrates is caused by the surface plasmon resonances (SPR) of the silver nanoparticles (Figure 1c).[53] The maximum absorption occurred at a longer wavelength compared to the SPR of a single nanoparticle (420 nm for silver nanoparticles of 30 nm diameter in solution)[54] suggesting the formation of silver nanoparticle aggregates, which was indeed confirmed by SEM images (Figure 1a). The UV–vis absorption spectra of the SERS substrates of varying pore size overlap with the excitation wavelength of the incident light thus providing efficient conditions for 514 nm excitation.[55] On the other hand, the transmission of light through the SERS substrates is the highest in the near-IR range and remains high in the visible region (Figure 1d). SERS substrates with 355 nm pore diameters show the highest transmission in the visible region, around 50% at the excitation wavelength of 514 nm. The reflectance spectra of the neat PAMs (Figure S4, SI) show almost identical reflectivities irrespective of the pore diameters and thus no calibration was done in the Raman measurements.

The SERS activity of the substrates was tested using BT as the Raman marker.[56] The SERS activity of the substrates was found to increase dramatically as the pore diameter was increased from 100 to 355 nm as evidenced by the rise in relative intensity of the characteristic Raman peaks of the BT

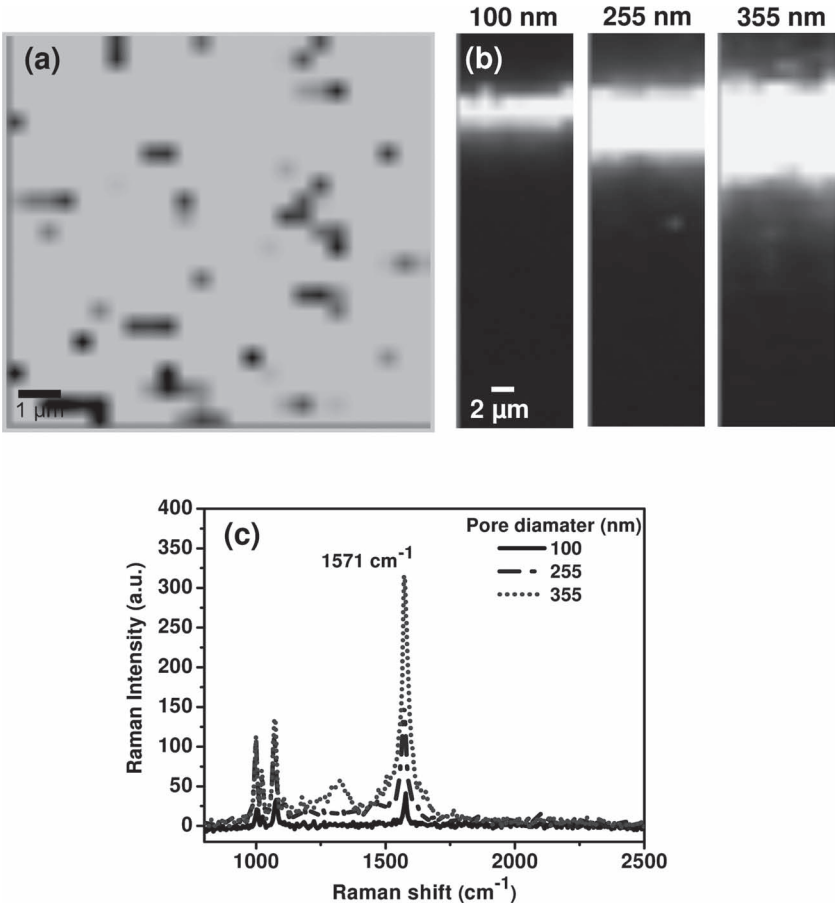

Figure 2. a) Surface (*x*,*y*) Raman mapping of the 1571 cm^{-1} peak of BT for substrates with 355 nm pore diameters. b) Confocal SERS mapping of the 1571 cm^{-1} peak of 10^{-6} M BT through the depth of the PAM with different pore diameters (pore dimension is shown on the corresponding *z* profile). c) SERS spectra of BT obtained at ~5 μm depth of the PAM-based SERS substrates.

molecules (Figure S5, SI). To understand the enhancement pattern we elucidated the 3D distribution of SERS activity in the cylindrical pores by conducting complete Raman mapping in both the (*x*,*y*) plane and *z* direction (**Figure 2**a,b). The mapping was conducted by monitoring the intensity of the 1571 cm^{-1} peak (caused by symmetric C–C stretching of BT) through the depth of the nanopores. The (*x*,*y*) distribution of the SERS signal for a 10 μm × 10 μm surface collected for pore diameters of 355 nm is presented in Figure 2a. As apparent from the 2D Raman map, a uniform SERS enhancement occurs over the entire region of the substrate, wherein the SERS intensity varies slightly from pore to pore (±25%).

To further check the macroscopic uniformity of the SERS substrates both within a sample and between different batches, the SERS activity from different positions (at least 10 positions) on multiple substrates of the same pore diameter (355 nm) was measured for a laser footprint below 1 μm across (Figure S6, SI). The SERS intensity was found to be very reproducible at different locations within a substrate and from different substrates (±7%), which indicates a high degree of homogeneity in the SERS substrates despite local variations in the aggregated morphology and the presence of residual seeds.

On the other hand, *z* mapping of the SERS activity of different nanopores shows that the largest SERS enhancement occurs within the first 10 μm beneath the membrane surface (Figure 2b). The SERS intensity of the BT signal gradually decreases as the depth increases for all pore diameters. SERS spectra of BT obtained at approximately 5 μm depth show consistent spectra with diminishing Raman band intensity (Figure 2c). To confirm the presence of a BT surface layer in the SERS substrates, fractured SERS substrates (cross-sections) were analyzed using X-ray photoelectron spectroscopy (XPS). Quantitative estimation of surface coverage was found to be impossible because of inhomogeneities in the fractured surface structure. However, signals corresponding to BT were detected from the fractured samples (Figure S7, SI).

The electromagnetic SERS enhancement through the cylindrical pores was further simulated by using silver nanoparticle dimers placed at various depths (see SI). Silver nanoparticle dimers were selected to reflect the common geometry of aggregates inside the pores. The dimers were placed in the pores with an orientation that provided a maximum enhancement between the nanoparticles (see the hot spot in **Figure 3**a). Dimers are selected because this is the predominant type of aggregate (see Figure S3, SI). Dimers with other orientations and separations provide minor contributions. The modeling we have performed is limited to two dimensions. Therefore, aggregates larger than dimers were not modelled because there is no way to arrange particles in 2D and create a larger enhancement than that of two particles. Even in 3D it is difficult to arrange spherical particles so more than two touch in any one location. To have three or more nanoparticles meeting at a single location requires non-ideal particles (i.e., non spherical particles). The enhancement predicted here corresponds to the enhancement levels reported earlier for silver dimers.[57,58]

These simulations showed that the cylindrical pore acts to constrain the incident radiation in a manner such that the maximum enhancements can be realized at a certain pore diameter and at a certain depth (Figure 3b). As the pore diameter increases the electric field in the inter-particle gap increases and the highest field intensity is achieved for about a 400 nm pore diameter. Moreover, a series of electromagnetic field peak intensities are observed along the main axis of the cylindrical pores with spacing close to $\lambda/2$. It is also evident from Figure 3b that a significant electromagnetic enhancement occurs for nanoparticle dimers placed continuously at several microns beneath the surface, which is in good agreement with the experimental *z*-mapping of the

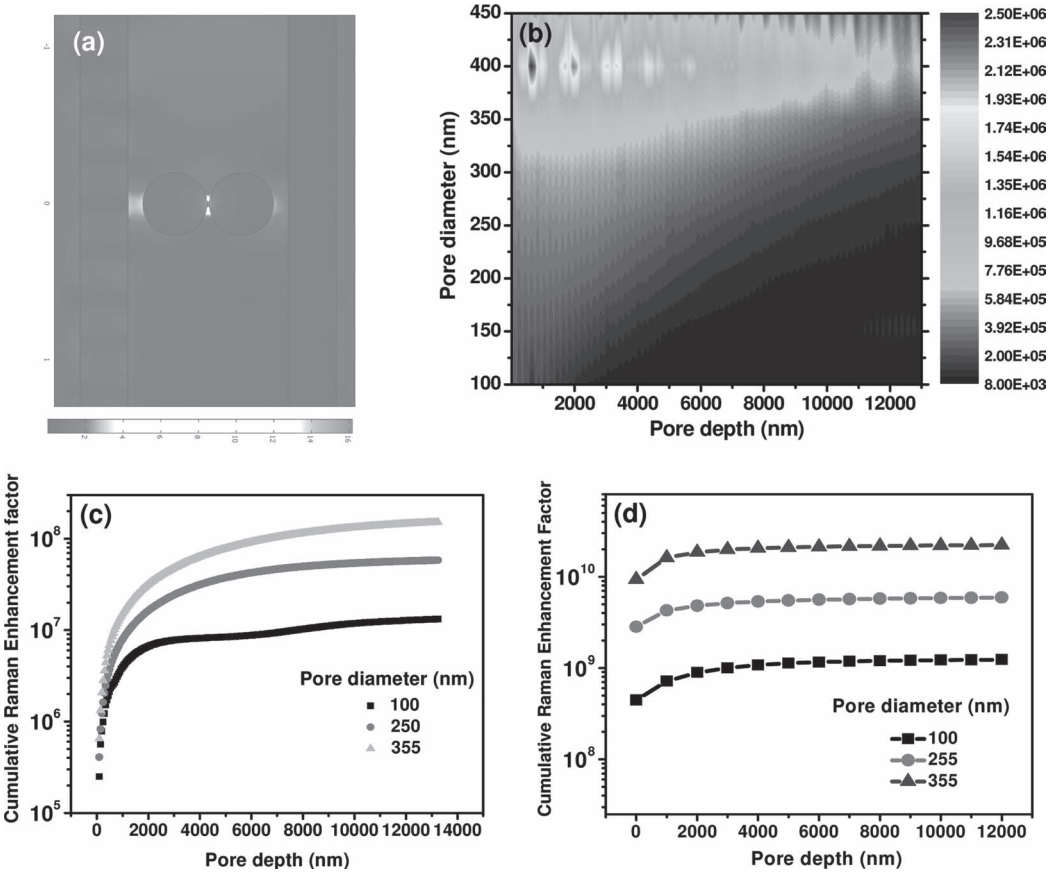

Figure 3. a) Electric field distribution for a silver nanoparticle dimer with a separation of 1.5 nm placed in an alumina membrane with pore diameter of 100 nm. The nanoparticles were excited by 514 nm light from the top of the pore with a polarization parallel to the long axis of the dimer. b) Simulated electrical field intensity distribution for a silver nanoparticle dimer as a function of pore diameter and depth. c) Variation in the simulated Raman enhancement factor (cumulative) for different pore diameters (100, 250, and 350 nm) at increasing pore depths. d) Cumulative Raman enhancement factor extracted from the experimental z-mapping as a function of pore depth.

enhancement factor (Figure 2b). The Raman enhancement factor gradually increases with the accumulated addition of nanoparticle dimers with increasing pore depths (Figure 3c). The simulated accumulated enhancement factor shows a saturation at depths higher than 10 μm. Consistent with simulations, experimental observations confirmed that the membranes with 355 nm pore diameters displayed increasing SERS activity with saturation at depths of 10–14 μm (Figure 3d). For the direct calculation of the experimental enhancement factor we utilized a common approach that compares the intensities of major Raman bands for solutions of known concentrations with and without the SERS substrate. This method assumes that all molecules in the solution migrate to the substrate in the course of solvent evaporation (see SI for details on the enhancement factor calculation).[59] It is commonly known that this method underestimates the actual enhancement because only a fraction of the molecules from the solution actually end up on the silver nanoparticles despite the higher affinity to thiolated analytes. Thus, the number reported here represents a lower bound, which can in fact be many-fold higher. But even this lower bound value is significantly higher than that reported for ordered microfabricated lithographical SERS substrates with average values around 10^7, with a highest enhancement factor of 10^9 reported for a localized region without averaging over the total surface or volume.[38,41,60–62]

The general behavior for all pore diameters is similar, but the 355 nm pores show the highest enhancement factor, which is an order of magnitude higher than that obtained for substrates with 100 nm pore diameters. As clear from the data, the general trends observed in the experiments and obtained from the simulations are similar considering the limited *z*-resolution of the Raman mapping (~1 μm). However, the experimental enhancement factor is more than two orders of magnitude higher than that calculated from the simulation of the electromagnetic field distribution. This increase can be attributed to the additional contribution from chemical enhancement (which can reach 10^3) for benzenethiol molecules chemisorbed on the silver nanoparticles, which is not accounted for in the simulation.[63]

Considering both experimental data from the *z*-distribution of Raman scattering and the simulated results on the electromagnetic field distribution for PAMs decorated with silver nanoparticles we can conclude that the optimization of Raman activity for long cylindrical pores can be achieved by choosing a pore diameter of around 350–400 nm and a total depth of 10–14 μm. Overall, the current study provides an example of a comprehensive approach that considers

the transmission of light and the aggregation of nanoparticles confined in cylindrical pores toward designing highly optimized 3D SERS substrates with enhancement factors several orders of magnitude higher than those of traditional planar substrates or non-optimized porous substrates. Such an approach provides an efficient pathway for the further development of nanoporous and holey designs, which can allow the detection of trace concentrations of practical target molecules with low Raman cross-sections such as explosives, hazardous chemicals, gases, and biomarkers.

Supporting Information

Supporting Information is available from the Wiley Online Library or from the author.

Acknowledgements

Financial support from NSF-CBET 0930781, and a DARPA/US Army SBIR W31P4Q10C0027 out of AMRDEC Weapons Science Directorate (WSD) through a subcontract from EngeniusMicro are acknowledged with gratitude. Z. A. Combs thanks the National Defense Science and Engineering Graduate (NDSEG) Fellowship, 32 CFR 168a. We also thank Richard Davis and Swati Naik for their help in the initial stages of this study.

[1] *Surface-Enhanced Raman Scattering Physics and Application*. (Eds: K. Kneipp, M. Moskovits, H. Kneipp), Springer, New York, **2006**.
[2] S. Schlucker, *Surface Enhanced Raman Spectroscopy: Analytical, Biophysical and Life Science Applications*, Wiley-VCH GmbH, Weinheim, Germany **2011**.
[3] G. A. Baker, D. S. Moore, *Anal. Bioanal. Chem.* **2005**, *382*, 1751.
[4] S. J. Lee, M. Moskovits, *Nano Lett.* **2011**, *11*, 145.
[5] K. Kneipp, H. Kneipp, I. Itzkan, R. R. Dasari, M. S. Feld, *Chem. Rev.* **1999**, *99*, 2957.
[6] C. Jiang, W. Y. Lio, V. V. Tsukruk, *Phys. Rev. Lett.* **2005**, *95*, 115503.
[7] E. Kharlampieva, T. Tsukruk, J. M. Slocik, H. Ko, N. Poulsen, R. R. Naik, N. Kröger, V. V. Tsukruk, *Adv. Mater.* **2008**, *20*, 3279.
[8] S. Singamaneni, E. Kharlampieva, J.-H. Jang, M. E. McConney, H. Jiang, T. J. Bunning, E. L. Thomas, V. V. Tsukruk, *Adv. Mater.* **2010**, *22*, 1369.
[9] S. M. Nie, S. R. Emory, *Science* **1997**, *275*, 1102.
[10] K. Kneipp, Y. Wang, H. Kneipp, L. T. Perelman, I. Itskan, R. R. Dasari, M. S. Feld, *Phys. Rev. Lett.* **1997**, *78*, 1667.
[11] J. P. Camden, J. A. Dieringer, Y. Wang, D. J. Masiello, L. D. Marks, G. C. Schatz, R. P. Van Duyne, *J. Am. Chem. Soc.* **2008**, *130*, 12616.
[12] K. Kneipp, H. Kneipp, G. Deinum, I. Itzkan, R. R. Dasari, M. S. Feld, *Appl. Spectrosc.* **1998**, *52*, 175.
[13] S. L. Kleinman, E. Ringe, N. Valley, K. L. Wustholz, E. Phillips, K. A. Scheidt, G. C. Schatz, R. P. Van Duyne, *J. Am. Chem. Soc.* **2011**, *133*, 4115.
[14] R. G. Freeman, K. C. Grabar, K. J. Allison, R. M. Bright, J. A. Davis, A. P. Guthrie, M. B. Hommer, M. A. Jackson, P. C. Smith, D. G. Walter, M. J. Natan, *Science* **1995**, 267, 1629.
[15] Z. Wang, S. Pan, T. D. Krauss, H. Du, L. J. Rothberg, *Proc. Natl. Acad. Sci. USA* **2003**, *100*, 8638.
[16] C. H. Lee, L. Tian, S. Singamaneni, *ACS Appl. Mater. Interfaces* **2010**, *2*, 3429.
[17] Z. A. Combs, S. Chang, T. Clark, S. Singamaneni, K. D. Anderson, V. V. Tsukruk, *Langmuir* **2011**, *27*, 3198.
[18] S. Chang, H. Ko, R. Gunawidjaja, V. V. Tsukruk, *J. Phys. Chem. C.* **2011**, *115*, 4387.
[19] M. J. Banholzer, J. E. Millstone, L. D. Qin, C. A. Mirkin, *Chem. Society Reviews* **2008**, *37*, 885.
[20] J. C. Hulteen, D. A. Treichel, M. T. Smith, M. L. Duval, T. R. Jensen, R. P. Van Duyne, *J. Phys. Chem. B* **1999**, *103*, 3854.
[21] R. Gunawidjaja, S. Peleshanko, H. Ko, V. V. Tsukruk, *Adv. Mater.* **2008**, *20*, 1544.
[22] L. Qin, S. Zhou, C. Xue, A. Atkinson, G. C. Schatz, C. A. Mirkin, *Proc. Natl. Acad. Sci. U.S.A* **2006**, *103*, 13300.
[23] A. M. Gobin, M. H. Lee, N. J. Halas, W. D. James, R. A. Drezek, J. L. West, *Nano Lett.* **2007**, *7*, 1929.
[24] M. K. Gupta, S. Chang, S. Singamaneni, L. F. Drummy, R. Gunawidjaja, R. R. Naik, V. V. Tsukruk, *Small* **2011**, *7*, 1192.
[25] S. Chan, S. Kwon, T. Koo, L. Lee, A. A. Berlin, *Adv. Mater.* **2003**, *15*, 1595.
[26] H. Ko, S. Singamaneni, V. V. Tsukruk, *Small* **2008**, *4*, 1576.
[27] L. H. Qian, Y. Ding, T. Fujita, M. W. Chen, *Langmuir* **2008**, *24*, 4427.
[28] H. He, W. Cai, Y. Lin, B. Chen, *Chem. Commun.* **2010**, *46*, 7223.
[29] H. Ko, V. V. Tsukruk, *Small* **2008**, *4*, 1980.
[30] S. Chang, H. Ko, S. Singamaneni, R. Gunawidjaja, V. V. Tsukruk, *Anal. Chem.* **2009**, *81*, 5740.
[31] P. M. Tessier, O. D. Velev, A. T. Kalambur, A. M. Lenhoff, J. F. Rabolt, E. W. Kaler, *Adv. Mater.* **2001**, *13*, 396.
[32] P. M. Tessier, O. D. Velev, A. T. Kalambur, J. F. Rabolt, A. M. Lennhoff, E. W. Kaler, *J. Am. Chem. Soc.* **2000**, *122*, 9554.
[33] P. Xu, N. H. Mack, S. H. Jeon, S. K. Doorn, X. Han, H. L. Wang, *Langmuir* **2010**, *26*, 8882.
[34] A. Amezcua-Correra, J. Yang, C. E. Finlayson, A. C. Peacock, J. R. Hayes, P. J. A. Sazio, J. J. Baumberg, S. M. Howdle, *Adv. Funct. Mater.* **2007**, *17*, 2024.
[35] T. L. Williamson, X. Guo, A. Zukoski, A. Sood, D. J. Diaz, P. W. Bohn, *J. Phys. Chem. B* **2005**, *109*, 20186.
[36] A. G. Brolo, E. Arctander, R. Gordon, B. Leathem, K. L. Kavanagh, *Nano Lett.* **2004**, *4*, 2015.
[37] H. Ko, S. Chang, V. V. Tsukruk, *ACS Nano* **2009**, *3*, 181.
[38] L. B. Luo, Li. M. Chen, M. L. Zhang, Z. B. He, W. F. Zhang, G. D. Yuan, W. J. Zhang, S. T. Lee, *J. Phys. Chem. C* **2009**, *113*, 9191.
[39] M. Kahl, E. Voges, S. Kostrewa, C. Viets, W. Hill, *Sens. Actuator A-Phys.* **1998**, *51*, 285.
[40] P. M. Tessier, O.D. Velev, A. T. Kalambur, J. F. Rabolt, A. M. Lenhoff, E. W. Kaler. *J. Am. Chem. Soc.* **2000**, *122*, 9554.
[41] M. Fan, G. F.S. Andrade, A. G. Brolo, *Anal. Chim. Acta* **2011**, *693*, 7.
[42] M. Saito, M. Shibasaki, S. Nakamura, M. Miyagi, *Opt. Lett.* **1994**, *19*, 710.
[43] K. H. A. Lau, S. Tan, K. Tamada, M. S. Sander, W. J. Knoll, *Phys. Chem. B.* **2004**, *108*, 10812.
[44] Y. Du, L. Shi, T. He, X. Sun, Y. Mo, *Appl. Surf. Sci.* **2008**, *255*, 1901.
[45] R. J. Walsh, G. Chumanov, *Appl. Spectrosc.* **2001**, *55*, 1695.
[46] B. Mondal, S. K. Saha, *Chem. Phys. Lett.* **2010**, *497*, 89.
[47] N. Ji, W. Ruan, C. Wang, Z. Lu, B. Zhao, *Langmuir* **2009**, *25*, 11869.
[48] R. L. Aggarwal, L. W. Farrar, E. D. Diebold, L. J. Polla, *Raman Spectrosc.* **2009**, *40*, 1331.
[49] B. M. Zamuner, D. Talaga, F. Deiss, V. Guieu, A. Kuhn, P. Ugo, N. Sojic, *Adv. Funct. Mater.* **2009**, *19*, 3129.

[50] C. H. Sun, N. C. Linn, P. Jiang, *Chem. Mater.* **2007**, *19*, 4551.
[51] H. Masuda, K. Fukuda, *Science* **1995**, *268*, 1466.
[52] A. P. Li, F. Müller, A. Birner, K. Nielsch, U. Gösele, *Adv. Mater.* **1999**, *11*, 483.
[53] S. Chang, Z. A. Combs, M. K. Gupta, R. Davis, V. V. Tsukruk, *ACS Appl. Mater. Interfaces* **2010**, *2*, 3339.
[54] D. D. Evanoff Jr., G. Chumanov, *ChemPhysChem* **2005**, *6*, 1221.
[55] C. L. Haynes, R. P. Van Duyne, *J. Phys. Chem. B* **2003**, *107*, 7426.
[56] S. J. Lee, A. R. Morrill, M. Moskovits, *J. Am. Chem. Soc.* **2006**, *128*, 2200.
[57] R. J. C. Brown, J. Wang, R. Tantra, R. E. Yardley, M. J. T. Milton, *Faraday Discussions* **2006**, *132*, 201.
[58] Z. Q. Tian, B. Ren, *J. Phys. Chem. B* **2002**, *106*, 9463.
[59] E. C. Le Ru, P. G. Etchegoin, *Principles of Surface-Enhanced Raman Spectroscopy and Related Plasmonic Effects*, Elsevier, New York, **2009**.
[60] H. Im, K. C. Bantz, N. C. Lindquist, C. L. Hynes, S. H. Oh, *Nano Lett.* **2010**, *10*, 2231.
[61] S. M. Wells, S. D. Retterer, J. M. Oran, M. J. Sepaniak, *ACS Nano* **2009**, *3*, 3845.
[62] A. Gopinath, S. V. Boriskina, W. R. Premasiri, L. Ziegler, B. M. Reinhard, L. D. Negro, *Nano Lett.* **2009**, *9*, 3922.
[63] S. K. Saikin, R. O. Amaya, D. Rappoport, M. Stopa, A. A. Guzik, *Phys. Chem. Chem. Phys.* **2009**, *11*, 9401.

Received: September 19, 2011
Published online: November 4, 2011